Theoretical study on HNC($^1\Sigma$) production from the $C_2(X^1\Sigma_g^+)$ + $NH(X^3\Sigma^-)$ reaction

Kenta Takahashi and Toshiyuki Takayanagi*

Department of Chemistry, Saitama University, 255 Shimo-Okubo, Sakura-ku, Saitama City, Saitama 338-8570, Japan

Abstract

The mechanism and dynamics of the reaction of $C_2(X^1\Sigma_g^+)$ with $NH(X^3\Sigma^-)$ have been investigated using electronic structure methods. The CASPT2 calculations show that C_2 can add to NH without a barrier. Several intermediates involved in the reaction on the lowest triplet potential energy surface were optimized at the B3LYP level and then the potential energy diagram was refined at more accurate levels of theory. In order to understand the reaction dynamics more quantitatively, direct dynamics calculations have been performed at the B3LYP level. It has been found that the HNC molecule is efficiently produced from the C_2 + NH reaction.

---

* Corresponding author.

E-mail address: tako@chem.saitama-u.ac.jp (T. Takayanagi)

1. Introduction

It is widely known that the abundance ratio of HNC/HCN in many interstellar sources is observed to be of the order of 1-1/100 [1-5]. Since HNC is thermochemically less stable than HCN by 14 kcal/mol [6], the observed abundance ratio cannot totally be explained by thermal equilibrium and this finding has attracted much attention for recent years. In order to explain such thermochemically unrealistic abundances in the interstellar clouds, several chemical reactions have been suggested that are capable of forming HNC/HCN products. Among them, it has been widely accepted that the $HCNH^+$ cation, which has been detected in the interstellar space by spectroscopic techniques, is the major precursor of the HCN/HNC production since this cation recombines with an electron to reach both the H + HCN and H + HNC channels with the branching ratio being nearly unity [7-10]. In addition to this dissociative recombination of $HCNH^+$, it has been suggested that the neutral-neutral reaction, $C(^3P) + NH_2(^2B_1)$, may also play a role in the HNC production [11-14].

In this paper, we study the HNC production dynamics through the $C_2(X^1\Sigma_g^+) + NH(X^3\Sigma^-)$ reaction from a theoretical point of view. It is well known that the dicarbon molecule, C_2, in its ground electronic state has high reactivity and is playing an important role in high-temperature hydrocarbon flames as well as chemical vapor deposition of diamond [15-18]. In addition, the C_2 molecule has been detected in the interstellar medium [19,20] in carbon stars like IRC + 10216. Therefore, understanding the mechanism and dynamics of reactions of C_2 with various molecules is very important from a viewpoint of interstellar chemistry. For example, Kaiser and his co-workers have extensively studied the reactions of C_2 with unsaturated hydrocarbons [21,22] and H_2S [23] using a sophisticated crossed molecular beam method combined with electronic structure calculations. They have succeeded in identifying reaction products using mass spectroscopic techniques. In addition, rate constants for reactions of C_2 with simple molecules have been measured in a very low-temperature region and those rate constants are employed to understand the importance in the interstellar clouds [24]. As far as we are aware, the $C_2(X^1\Sigma_g^+) + NH(X^3\Sigma^-)$ reaction has not yet been studied from the experimental side or theoretical side. This is presumably because the $C_2(X^1\Sigma_g^+) + NH(X^3\Sigma^-)$ reaction is a radical-radical type reaction, which is

relatively difficult to be studied experimentally. However, it should be mentioned that theoretical studies based on electronic structure calculations and reaction dynamics calculations would be quite useful especially for such chemical reactions. In the following sections we will theoretically show that the $C_2(X^1\Sigma_g^+)$ + $NH(X^3\Sigma^-)$ reaction effectively produces the HNC molecule. We hope that the present study stimulate future experimental studies for understanding the HNC production mechanism in the dense interstellar clouds.

2. Computational Method

Geometries of reactants, products, intermediates, and transition-states on the lowest triplet potential energy surface for the $C_2(X^1\Sigma_g^+)$ + $NH(X^3\Sigma^-)$ reaction have been optimized using the hybrid density-functional B3LYP method [25,26] with the 6-311++G(d, p) basis set. Harmonic vibrational frequencies were calculated at the same level of theory in order to characterize the optimized geometries as potential minima or saddle points as well as to obtain zero-point energy corrections. Relative energies were then refined by single-point energy calculations at the CCSD(T)/6-311++G(3df,3pd) and full-valence CASPT2/aug-cc-pVTZ levels of theory so the overall levels can be written as CCSD(T)/6-311++G(3df,3pd)//B3LYP/6-311++G(d, p) or CASPT2/aug-cc-pVTZ //B3LYP/6-311++G(d, p). All calculations were carried out using the Gaussian 03 [27] and Molpro 2002 [28] package programs.

Although the reaction energy diagram is quite useful for understanding the overall reaction mechanism, it is still insufficient for understanding reaction dynamics from a microscopic point of view. Of course, one can also obtain statistical information from the RRKM theory; however, dynamical aspects including product energy distributions cannot easily be uncovered when the reaction does not proceed statistically. In order to overcome this difficulty, we have performed direct trajectory calculations on the lowest triplet potential energy surface for C_2 + NH. The direct trajectory calculations were carried out at the B3LYP/6-311++G(d, p) level, which was determined by compromise of computational costs and the accuracy. We employed the BOMD (Born-Oppenheimer molecular dynamics) method implemented in the GAUSSIAN 03 package [27]. This method uses a fifth-order

polynomial fitted to the energy, gradient, and Hessian at each time step, and then the step size is taken to be much larger than the step size used in the normal method employing only the gradient information [29]. As will be shown later, B3LYP/6-311++G(d, p)-level potential energy curves along appropriate internal coordinates were systematically compared to the potential curves obtained at a more accurate level of theory: CASPT2(8_e,10_o)/cc-pVTZ. Notice that the active space as well as basis set are somewhat reduced from the full-valence calculations used in the single-point energy calculations to save computational time.

3. Results and discussion

Fig. 1 displays the energy diagram of the lowest potential energy surface involved in the reaction of $C_2(X^1\Sigma_g^+)$ with $NH(X^3\Sigma^-)$. In this energy diagram, the energy level of the $HNC(X^1\Sigma) + C(^3P)$ products are defined as zero. It is found that the C_2 + NH reactants have a relatively large energy indicating that both the HNC/HCN + C product channels have large available energies. The reaction of C_2 with NH firstly leads to the HNCC intermediate without an entrance barrier (shown later). This HNCC intermediate can directly dissociate into the HNC + C channel; however, it is seen that the isomerization process leading to the NCCH intermediate through TS1 has a somewhat low energy barrier. The NCCH intermediate can further isomerize into the CNCH intermediate through TS2 and TS3 and finally dissociate into $C(^3P)$ + $HCN(X^1\Sigma)$ having the lowest product channel in energy. A part of this energy diagram has previously been obtained at a somewhat lower CCSD(T)/6-311+G(d, p)//B3LYP/6-311+G(d, p) level of theory by Goldberg et al. [30] in their mass spectrometric study on the ionic [H,C_2,N] system. However, it should be emphasized that they did not consider any dissociation channels at all. We found that the present result at the CASPT2 level is in reasonably good agreement with their result within ca 5 kcal/mol.

Before presenting direct dynamics BOMD results, it should be important to demonstrate the feasibility to use the B3LYP/6-311++(d, p) level of theory in the dynamics calculations. Fig. 2(a) shows the potential energy curves as a function of the C-N distance obtained by the B3LYP and CASPT2 methods. In this plot, other internal coordinates were

fully optimized with respect to energy at the B3LYP level of theory. It is seen that there is no entrance barrier for the C_2 + NH reaction and that agreement between the two results is quite good. Figs. 2(b) and (c) show similar comparisons but for potential energy curves as a function of a different coordinate. Again, agreement between the B3LYP and CASPT2 results is seen to be good. It is interesting to notice that both the CCNH and CNCH intermediates can finally dissociate into the C + HNC and C + HCN product channels, respectively, without exit barriers.

In the present BOMD calculations, the initial distance between C_2 and NH was set to 4 Å and the initial geometries of C_2 and NH were set to the equilibrium distances. The vibrational energies of C_2 and NH were completely ignored for computational simplicity. This is somewhat unrealistic but its effect is expected to be small due to a very large available energy for the reaction. The relative translational energy was fixed to 10^{-3} kcal/mol (nearly zero). The initial orientation between C_2 and NH molecule was randomly generated and the impact parameter was also randomly chosen in the range of 0-4 Å. We have generated 277 initial conditions and then run the GAUSSIAN program for each condition. A typical integration time was found to be in the range of 150-300 fs depending on the nature of the trajectory. About 300 trajectories obviously do not allow good quality statistical sampling but it must be kept in mind that the computational cost of the direct trajectory calculations is high even at the B3LYP/6-311++G(d, p) level. In spite of this limitation, we believe that the present direct classical trajectory calculations give important information on the reaction dynamics.

Typical snapshots along the BOMD trajectory and the corresponding time-evolution of the potential energy are presented in Fig. 3. It is seen that the HNCC intermediate is readily formed in this trajectory, but its lifetime is found to be quite short (~ 30 fs). Since the C-N bond is firstly produced, it is reasonable that a large part of energy is partitioned into the C-N stretch vibration in an early stage. However, since the C-C-N geometry is nearly collinear and mass difference between N and C atoms is quite small, momentum transfer can easily occur between N and C. Therefore, the C-C bond rapture readily occurs and HNC + C is produced within very short time. This suggests that, when the initially formed HNCC intermediate has nearly its equilibrium structure, it is difficult that an available energy is

partitioned into the kinetic energy of the hydrogen atom. In other words, the isomerization process from the HNCC intermediate to HCCN via TS1 does not occur easily.

Table 1 summarizes the statistical result of our BOMD calculations. It was found that 342 trajectories lead to HNC + C implying that the branching fraction of this channel is about 97 %. Our simulations also show that 7 trajectories lead to the CNCH or CCNH intermediate, which did not dissociate into any products within 300 fs. From the present BOMD simulation, it is therefore concluded that the $C_2(X^1\Sigma_g^+)$ + $NH(X^3\Sigma^-)$ reaction quite effectively produces the HNC molecule. We have further analyzed the relative translational energy distribution between C + HNC as well as the internal (vibrational + rotational) energy distribution of HNC in order to understand the overall reaction dynamics more quantitatively. The result of this analysis is presented in Fig. 4 along with the average energy. The distribution of the relative translational energy has a peak at ~ 0 kcal/mol, showing a typical distribution for reactions with no exit barrier. From the energy conservation, this distribution gives that the internal energy distribution has a peak at a large value of ~ 64 kcal/mol. This indicates that a large part of the available energy for the HNC + C channel is partitioned into the internal energy of the HNC molecule. It should be emphasized that, since the isomerization barrier height from HNC to HCN is 33 kcal/mol, many trajectories lead to the fact that the product HNC molecule has an internal energy larger than this barrier. However, we found no trajectories for which further isomerization from HNC to HCN occurs within our simulation time. This indicates that the internal energy in HNC is mainly distributed in the CN stretch mode not in the kinetic energy of the H atom. Thus, only a small energy is partitioned into the CH stretch and bending mode although our analysis is fully based on a classical mechanics picture.

Finally, we would like to finally emphasize that theoretical studies such as quantum chemical calculations as well as reaction dynamics calculations play a very important role for understanding reactions for which modern experimental techniques are difficult to apply. Chemical reactions occurring in the interstellar clouds are definitely such cases because reactions take place at extremely low temperatures and under extremely low pressure conditions. Nevertheless, experimental investigation should be done in order to evaluate the accuracy of theoretical calculations. In particular, information on product branching is still

insufficient for many reaction systems and it should be important that experimental methods are developed that enable product branching ratios to be determined at very low temperatures. We believe that this kind of theoretical studies stimulate further development of new experimental techniques.

4. Conclusion and future direction

The present electronic structure calculations as well as direct dynamics calculations provide information on the efficient HNC production from the $C_2(X^1\Sigma_g^+)$ and $NH(X^3\Sigma^-)$ reaction. Our accurate ab initio calculations at the CASPT2 level show that there is no entrance barrier for the $C_2(X^1\Sigma_g^+)$ + $NH(X^3\Sigma^-)$ approach and no exit barrier for the dissociation process of HNCC $\rightarrow$ C + HNC on the lowest triplet potential energy surface. Since we have found that the B3LYP-level calculations give reasonable agreement with the CASPT2 potential energy surface, we have carried out direct dynamics BOMD calculations for understanding the reaction dynamics. It has been found that the HNC molecule is produced from the C_2 and NH reactants with very high efficiency. This should be the result of reaction dynamics on the potential energy surface, where the initially-formed HNCC intermediate has a nearly linear N-C-C structure; the initial available energy is largely partitioned into the newly-formed N-C stretch and then the energy is readily transferred into the C-C stretch.

In this work, we have studied the reaction dynamics only on the lowest triplet potential energy surface. However, previous ab initio calculations [30] show that the energy level of the lowest singlet potential energy surface is very close to that of the lowest triplet surface. This suggests that nonadiabatic transitions through spin-orbit couplings may play some roles in the $C_2(X^1\Sigma_g^+)$ + $NH(X^3\Sigma^-)$ reaction dynamics. The importance of the lowest singlet potential energy surface can also be predicted from the fact that the electronically excited $C_2(a^3\Pi_u)$ state is lying only 718 cm^{-1} above the $C_2(X^1\Sigma_g^+)$ ground state [24]. Further theoretical studies along this line and the determination of interstellar implication of these reactions are currently in progress in our laboratory.

References

[1] W. M. Irvine, F. P. Schloeb, Astrophys. J. 282 (1984) 516.

[2] A. Wooten, N. J. Evans, II, R. Snell, P. V. Bout, Astrophys. J. 225 (1978) L143.

[3] T. Hirota, S. Yamamoto, H, Mikami, M. Ohishi, Astrophys. J. 503 (1998) 717.

[4] C. M. Walmsley, J. Chem. Soc. Faraday Trans. 89 (1993) 2119.

[5] J. Semaniak, B. F. Minaev, A. M. Derkatch, F. Hellberg, A. Neau, S. Rosén, R. Thomas, M. Larsson, H. Danared, A. Paál, M. af Ugglas, Astrophys. J. Suppl. 135 (2001) 275.

[6] J. M. Bowman, B. Gazdy, J. A. Bentley, T. J. Lee, C. E. Dateo, J. Chem. Phys. 99 (1993) 308.

[7] Y. Shiba, T. Hirano, U. Nagashima, K. Ishii, J. Chem. Phys. 108 (1998) 698.

[8] T. Taketsugu, A. Tajima, K. Ishii, T. Hirano, Astrophys. J. 608 (2004) 323.

[9] K. Ishii, A. Tajima, T. Taketsugu, K. Yamashita, Astrophys. J. 636 (2006) 927.

[10] H. Tachikawa, Phys. Chem. Chem. Phys. 1 (1999) 4925.

[11] D. Talbi, Chem. Phys. Lett. 312 (1999) 291.

[12] D. Talbi, Chem. Phys. Lett. 313 (1999) 626.

[13] E. Herbst, R. Terzieva, D. Talbi, MNRAS, 311 (2000) 869.

[14] T. Takayanagi, T. Taketsugu, Chem. Phys. Lett. 417 (2006) 143.

[15] A. P. Baranovski, McDonalds, J. Phys. Chem. 66 (1977) 3300.

[16] W. Weltner, R. J. van Zee, Chem. Rev. 89 (1989) 1713.

[17] P. John, J. R. Rabeau, J. I. B. Wilson, Diamond Relat. Mater. 11 (2002) 608.

[18] G. P. Smith, C. Park, J. Schneiderman, J. Luque, Combust. Flame 141 (2005) 66.

[19] S. B. Yorka, Astrophys. J. 88 (1983) 1816.

[20] A. Crawford, M. J. Barlow, MNRAS 311 (2000) 370.

[21] R. I. Kaiser, N. Balucani, D. O. Charkin, A. M. Mebel, Chem. Phys. Lett. 382 (2003) 112.

[22] A. M. Mebel. V. V. Kislov, R. I. Kaiser, J. Phys. Chem. A 110 (2006) 2421.

[23] R. I. Kaiser, M. Yamada, Y. Osamura, J. Phys. Chem. A 106 (2002) 4825.

[24] A. Páramo, A. Canosa, S. D. Le Picard, I. R. Sims, J. Phys. Chem. A 111 (2006) 3121.

[25] A. D. Becke, J. Chem. Phys. 98 (1993) 5648.

[26] C. Lee, W. Yang, R. G. Parr, Phys. Rev. B 37 (1988) 785.

[27] M. J. Frisch, G. W. Trucks, H. B. Schlegel, G. E. Scuseria, M. A. Robb, J. R. Cheeseman, J. A. Montgomery, Jr., T. Vreven, K. N. Kudin, J. C. Burant, J. M. Millam, S. S. Iyengar, J. Tomasi, V. Barone, B. Mennucci, M. Cossi, G. Scalmani, N. Rega, G. A. Petersson, H. Nakatsuji, M. Hada, M. Ehara, K. Toyota, R. Fukuda, J. Hasegawa, M. Ishida, T. Nakajima, Y. Honda, O. Kitao, H. Nakai, M. Klene, X. Li, J. E. Knox, H. P. Hratchian, J. B. Cross, C. Adamo, J. Jaramillo, R. Gomperts, R. E. Stratmann, O. Yazyev, A. J. Austin, R. Cammi, C. Pomelli, J. W. Ochterski, P. Y. Ayala, K. Morokuma, G. A. Voth, P. Salvador, J. J. Dannenberg, V. G. Zakrzewski, S. Dapprich, A. D. Daniels, M. C. Strain, O. Farkas, D. K. Malick, A. D. Rabuck, K. Raghavachari, J. B. Foresman, J. V. Ortiz, Q. Cui, A. G. Baboul, S. Clifford, J. Cioslowski, B. B. Stefanov, G. Liu, A. Liashenko, P. Piskorz, I. Komaromi, R. L. Martin, D. J. Fox, T. Keith, M. A. Al-Laham, C. Y. Peng, A. Nanayakkara, M. Challacombe, P. M. W. Gill, B. Johnson, W. Chen, M. W. Wong, C. Gonzalez, and J. A. Pople, Gaussian 03, Revision C.02, Gaussian, Inc., Wallingford CT, 2004.

[28] MOLPRO, a package of ab initio programs, H.-J. Werner and P. J. Knowles, version 2002.1, R. D. Amos, A. Bernhardsson, A. Berning, P. Celani, D. L. Cooper, M. J. O. Deegan, A. J. Dobbyn, F. Eckert, C. Hampel, G. Hetzer, P. J. Knowles, T. Korona, R. Lindh, A. W. Lloyd, S. J. McNicholas, F. R. Manby, W. Meyer, M. E. Mura, A. Nicklass, P. Palmieri, R. Pitzer, G. Rauhut, M. Schütz, U. Schumann, H. Stoll, A. J. Stone, R. Tarroni, T. Thorsteinsson, and H.-J. Werner.

[29] J. M. Millam, V. Bakken, W. Chen, W. L. Hase, B. H. Schlegel, J. Chem. Phys. 111 (1999) 3800.

[30] N. Goldberg, A. Fiedler, and H. Schwarz J. Phys. Chem. 99 (1995) 15327.

Table 1

Results of direct trajectory calculations for the C_2 + NH reaction at the B3LYP/6-311++G(d, p) level of theory

Product channel	# of trajectories	Fraction (%)
HNC + C	333	97.4
CCNH	5	1.5
CNCH	2	0.6
CNC + H	1	0.3
CCN + H	1	0.3
Sum	342	100

Figure Captions

Fig. 1 Potential energy diagram for the $C_2(X^1\Sigma_g^+)$ + $NH(X^3\Sigma^-)$ reaction obtained from the present electronic structure calculations. The relative energies include zero-point corrections obtained from the B3LYP/6-311++G(d, p)-level calculations.

Fig. 2 CASPT2 and B3LYP potential energy curves as a function of the CN distance or CC distance for dissociation processes of CCNH $\rightarrow$ C_2 + NH (a), CCNH$\rightarrow$ C + CNH (b), and CNCH $\rightarrow$ C + NCH.

Fig. 3 Typical snapshots of molecular structure along a trajectory resulting HNC + C from the C_2 + NH reaction (a) and its corresponding time-evolution of the potential energy (b).

Fig. 4 Distributions of relative translational energy between HNC + C (a) and internal energy (vibrational + rotational) of the HNC product (b). Average energies are also shown.

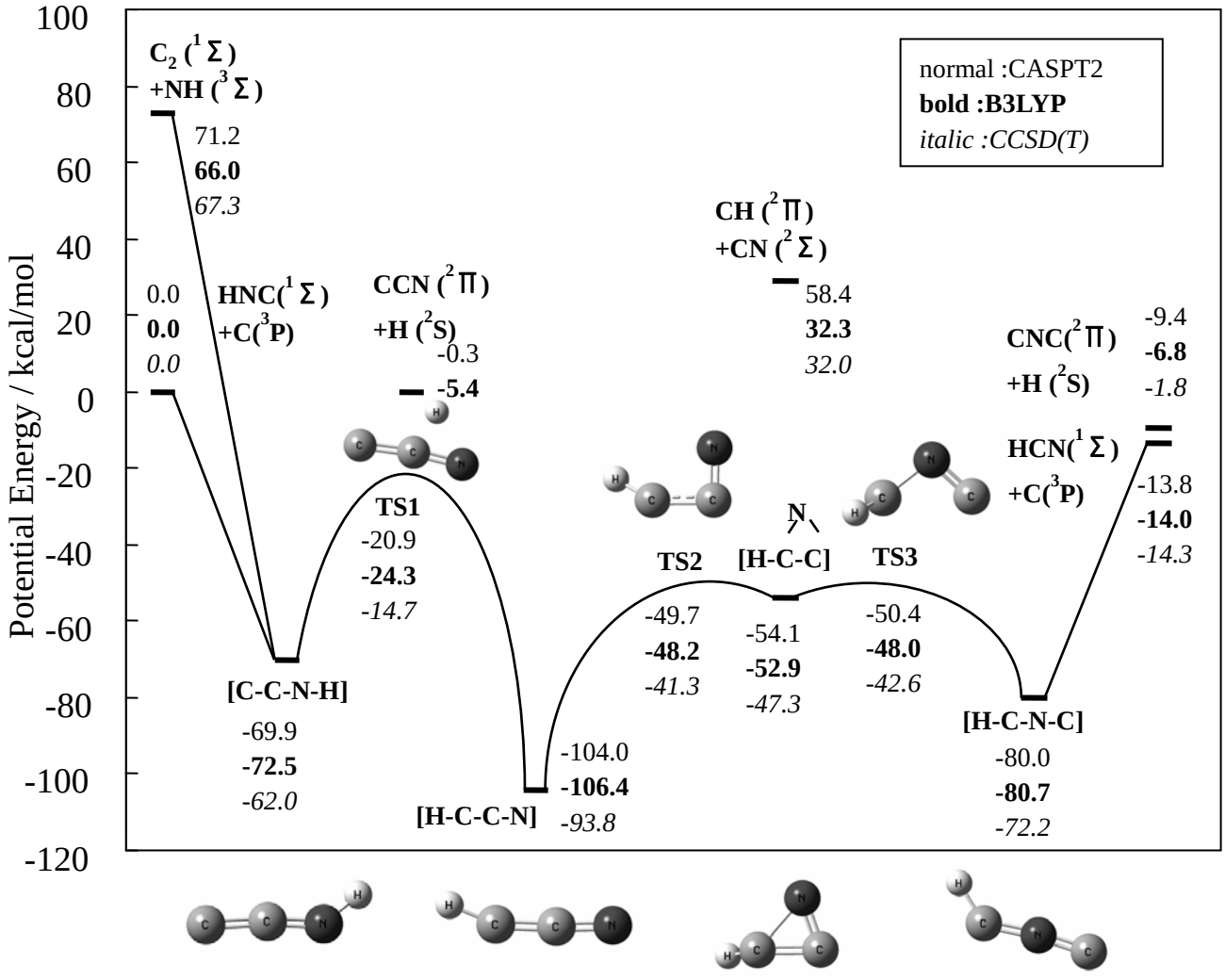
Potential Energy / kcal/mol
100
80
60
40
20
0
-20
-40
-60
-80
-100
-120
normal :CASPT2
bold :B3LYP
italic :CCSD(T)
C2 (1Σ)
+NH (3Σ)
71.2
66.0
67.3
0.0
0.0
0.0
HNC(1Σ)
+C(3P)
CCN (2Π)
+H (2S)
-0.3
-5.4
TS1
-20.9
-24.3
-14.7
[C-C-N-H]
-69.9
-72.5
-62.0
[H-C-C-N]
-104.0
-106.4
-93.8
CH (2Π)
+CN (2Σ)
58.4
32.3
32.0
TS2
-49.7
-48.2
-41.3
[H-C-C]
-54.1
-52.9
-47.3
TS3
-50.4
-48.0
-42.6
CNC(2Π)
+H (2S)
-9.4
-6.8
-1.8
HCN(1Σ)
+C(3P)
-13.8
-14.0
-14.3
[H-C-N-C]
-80.0
-80.7
-72.2

Figure 1

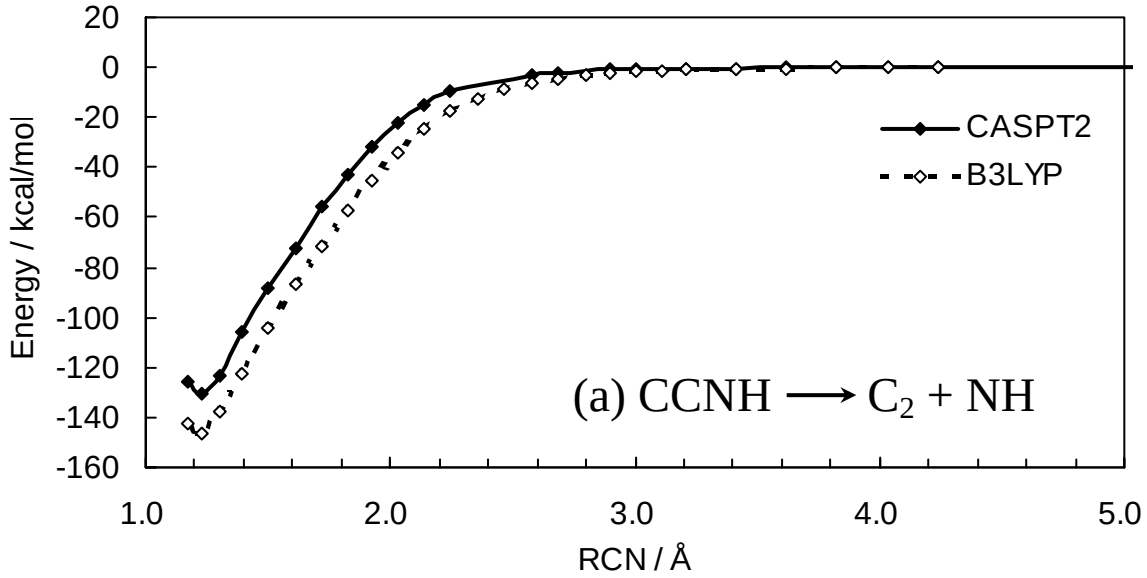
20
0
-20
-40
-60
-80
-100
-120
-140
-160
Energy / kcal/mol
CASPT2
B3LYP
(a) CCNH ⟶ C2 + NH
1.0
2.0
3.0
4.0
5.0
RCN / Å

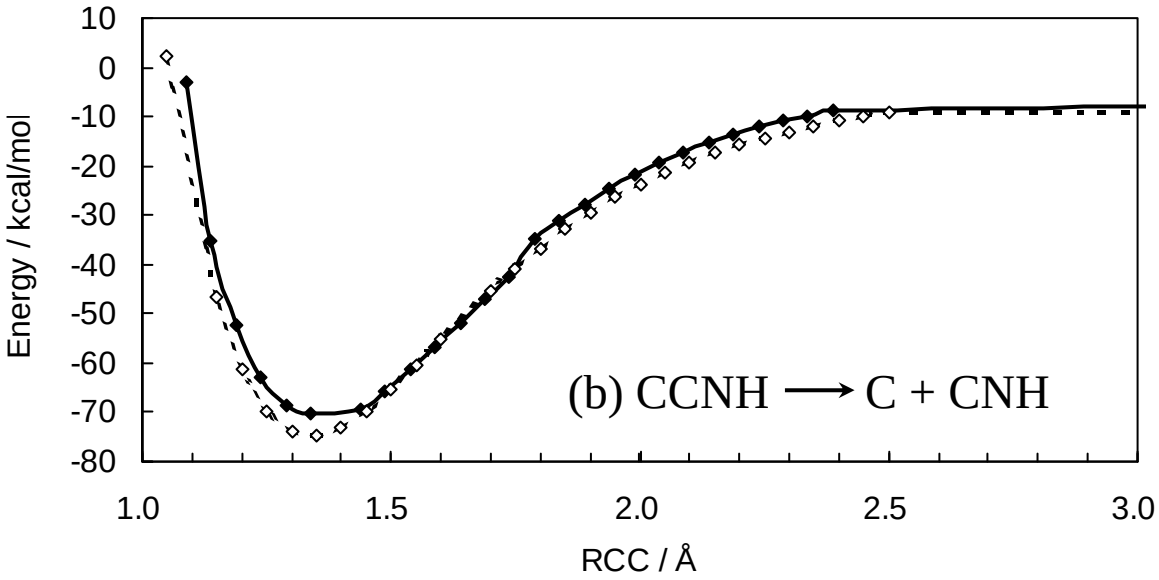
10
0
-10
-20
-30
-40
-50
-60
-70
-80
Energy / kcal/mol
(b) CCNH ⟶ C + CNH
1.0
1.5
2.0
2.5
3.0
RCC / Å

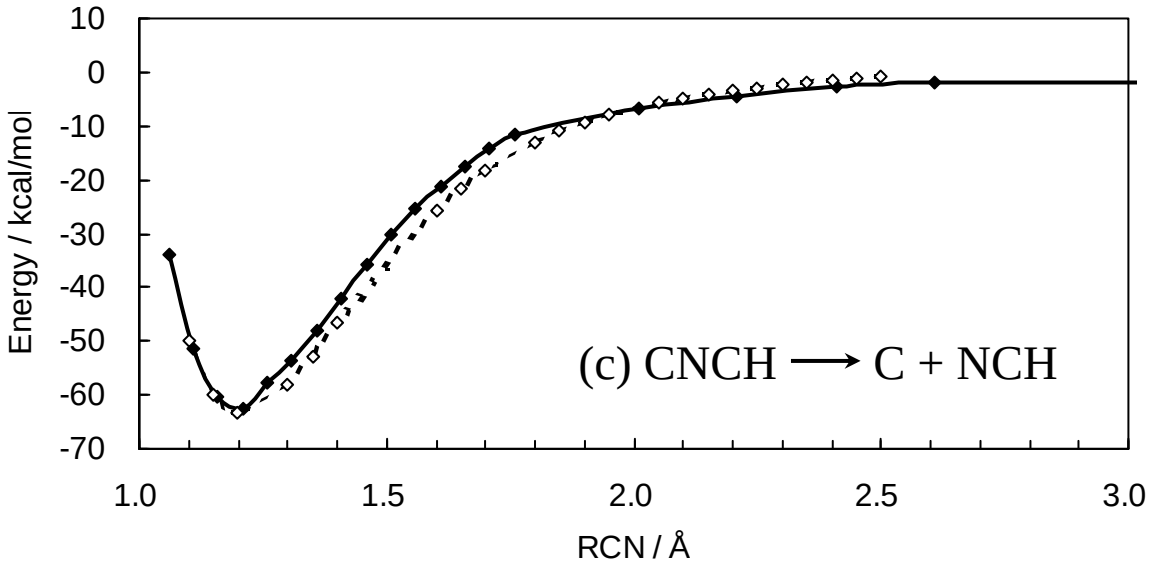
10
0
-10
-20
-30
-40
-50
-60
-70
Energy / kcal/mol
(c) CNCH ⟶ C + NCH
1.0
1.5
2.0
2.5
3.0
RCN / Å

Figure 2

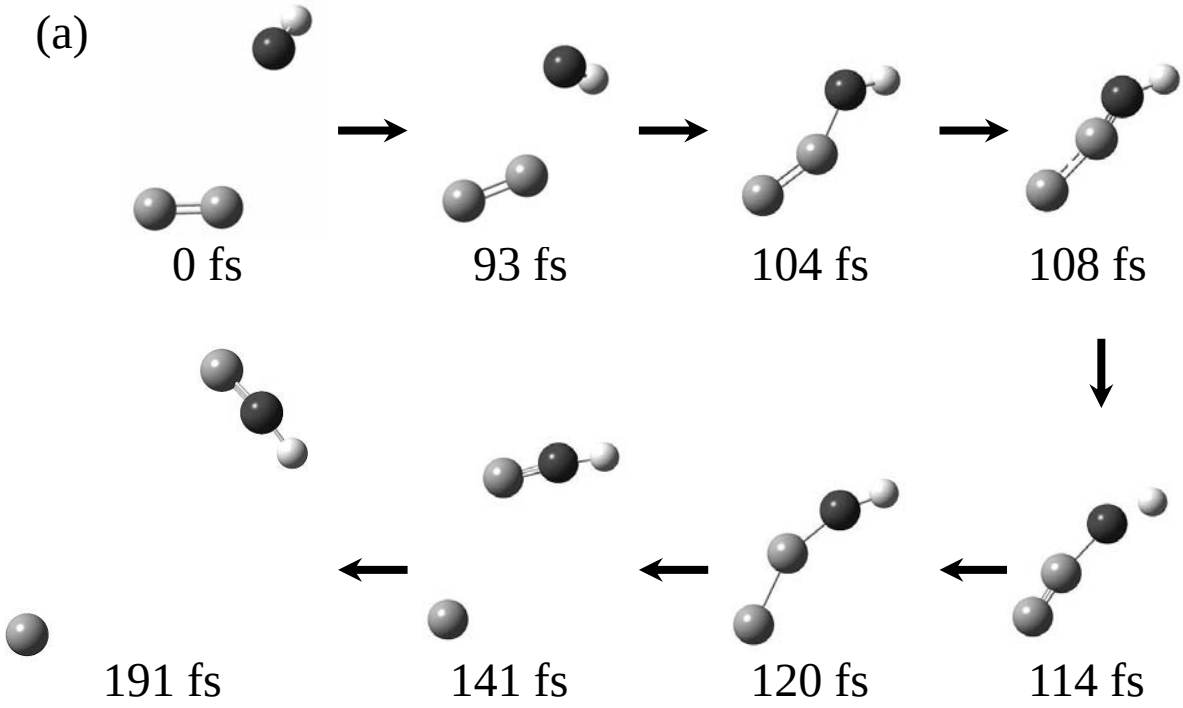
(a)
0 fs
93 fs
104 fs
108 fs
114 fs
120 fs
141 fs
191 fs

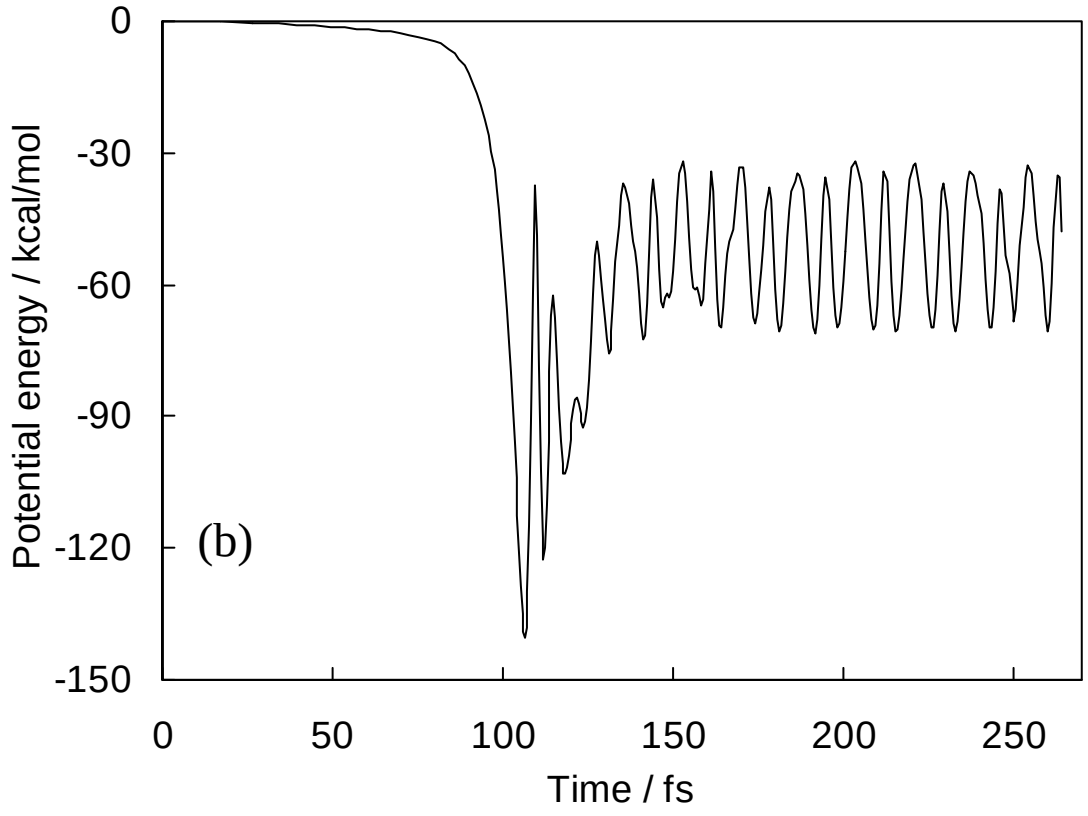
0
-30
-60
-90
-120
-150
Potential energy / kcal/mol
(b)
0
50
100
150
200
250
Time / fs

Figure 3

(a)

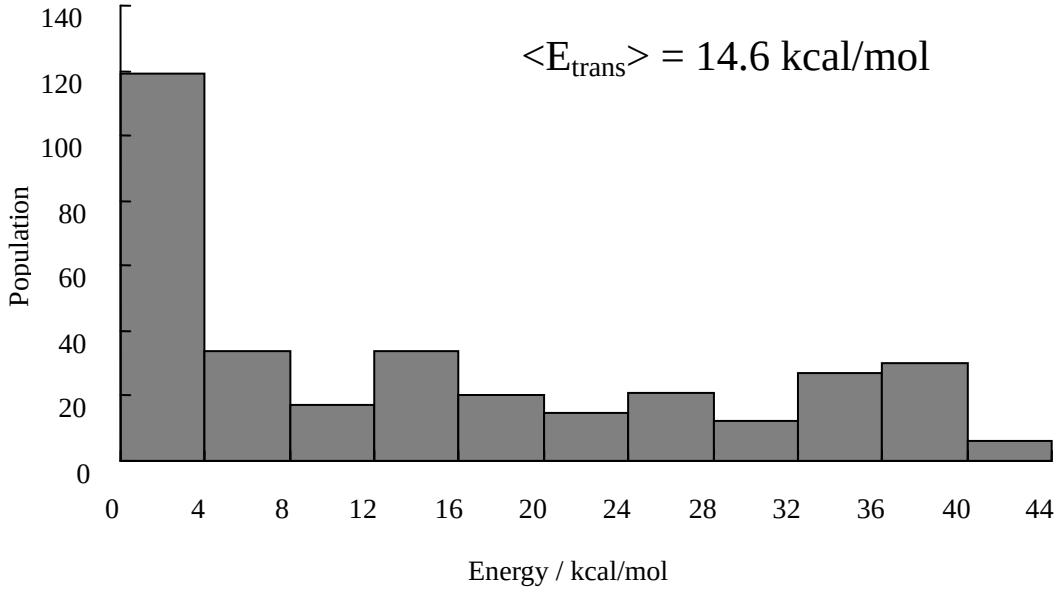
<E_trans> = 14.6 kcal/mol
Population
0
20
40
60
80
100
120
140
0
4
8
12
16
20
24
28
32
36
40
44
Energy / kcal/mol

(b)

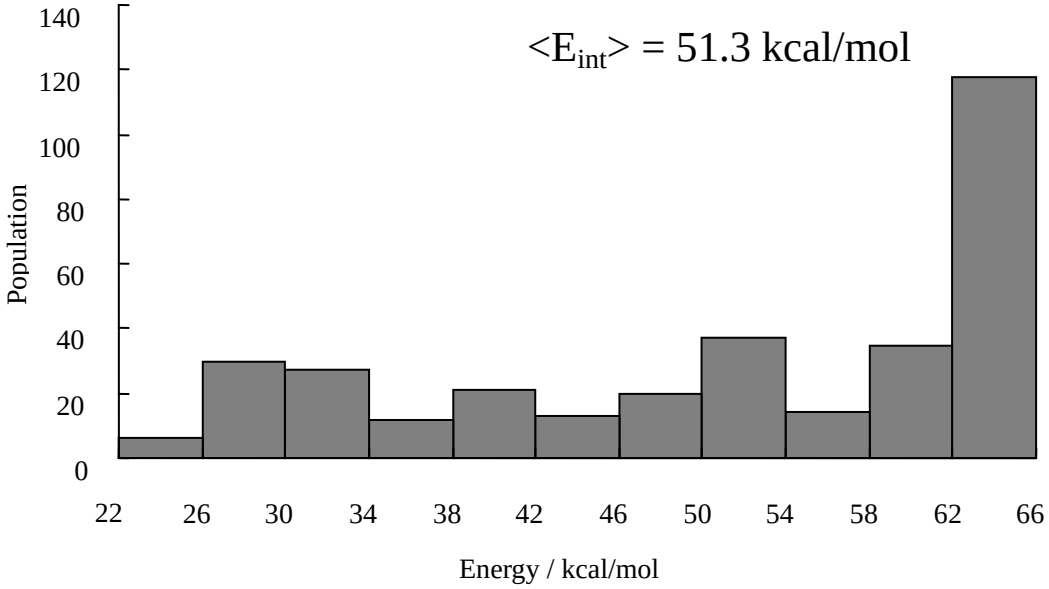
<E_int> = 51.3 kcal/mol
Population
0
20
40
60
80
100
120
140
22
26
30
34
38
42
46
50
54
58
62
66
Energy / kcal/mol

Figure 4